# INFLUENCE OF SYNTHESIS CONDITIONS ON THE OPTICAL PROPERTIES OF $Naregeo_4$ PHOSPHORS WITH OLIVINE STRUCTURE

**A. A. Melentsova[a], O. A. Lipina[a], A. Yu. Chufarov[a], A. P. Tyutyunnik[a], V. G. Zubkov[a]**

[a]*Institute of Solid State Chemistry of the Ural Branch of the Russian Academy of Sciences Ekaterinburg, 620990 Russia*
**e-mail: amelentsova@gmail.com*

Received July 16, 2024

Revised October 01, 2024
Accepted for publication October 02, 2024

Samples of $NaGdGeO_4$, $NaY_{0.975}Tm_{0.025}GeO_4$, $NaY_{0.975}Bi_{0.025}GeO_4$ and $NaY_{0.875}Bi_{0.025}Eu_{0.1}GeO_4$ were synthesized by various methods. According to powder X-ray diffraction data, the germanates crystallize in the orthorhombic system (space group *Pnma*, $Z = 4$). The influence of synthesis conditions on the surface characteristics and optical properties of the samples was evaluated, in particular, the samples were sintered under the action of thermal and microwave radiation, and the luminescent properties of the compounds were studied: $NaY_{0.975}Tm_{0.025}GeO_4$ - in the near-IR range (1100-2100 nm, $\lambda_{ex} = 808$ nm), $NaGdGeO_4$ - in the UV region (300-320 nm, $\lambda_{ex} = 257$ nm), $NaY_{0.975}Bi_{0.025}GeO_4$ and $NaY_{0.875}Bi_{0.025}Eu_{0.1}GeO_4$ - in the UV and visible wavelength range (300-700 nm, $\lambda_{ex} = 298$ nm). In the latter case, the influence of annealing conditions on the afterglow duration was additionally investigated.

*Keywords:* phosphors, olivines, microwave synthesis, optical properties, afterglow

**DOI:** 10.31857/S0044457X250101e8

## INTRODUCTION

Today, luminescent materials are an integral part of everyday life and are used as active optical components in various devices, namely: in LED-based lighting devices, displays [1], lasers [2, 3], motion and temperature sensors [4-6], as well as additives in the creation of special coatings [7].

The synthesis of modern phosphors is based on doping various optical matrices (both organic and inorganic) with rare earth element ions ( **REI** ). The high cost of

initial reagents and significant energy consumption of the technology for producing many promising luminescent materials make their industrial production impractical. A possible solution is to optimize the synthesis by reducing the temperature and annealing time, which leads to a reduction in electricity costs and has a positive effect on the final production cost. Since the genesis of a system determines its functioning, it is important to preserve the useful properties of materials when changing synthesis conditions; in the case of phosphors, such a property is high luminescence intensity. The use of microwave annealing may be a promising direction [8].

Heating of dielectrics in microwave ovens occurs due to the release of heat resulting from dielectric losses during polarization. Under the influence of an external electromagnetic field, intermolecular interaction occurs due to forced oscillations of polar molecules, which leads to heat release throughout the dielectric. Thus, the heating temperature of the latter is directly related to the average kinetic energy of atoms or molecules, which increases in proportion to the power of microwave radiation exposure. The absence of direct contact between the sample and the heater contributes to more uniform heating of the material throughout the volume [9] and advantageously distinguishes this annealing method from traditional ones. The advantages of microwave annealing also include high sintering speed, low thermal inertia, and significantly smaller crystallite size of the final products [10-12]. The latter is associated with the enhancement of grain boundary diffusion, leading to the predominance of densification processes through the removal of open porosity over grain growth processes.

In work [13], microwave annealing was successfully used to obtain phosphors with the olivine structure $NaYb_{1-x}Er_xGeO_4$ and $NaY_{1-y}Yb_{3y/4}Er_{y/4}GeO_4$, which exhibit luminescence in the visible range. However, the authors did not present an assessment of the influence of the synthesis and annealing method on the optical characteristics of such materials, which became the main goal of this work.

The choice of germanates $NaREGeO_4$ (RE = Y, Gd), belonging to the olivine structural type, as optical matrices is due to the possibility of creating phosphors with intense emission in a wide range of wavelengths (from UV to IR range) [14, 15] by doping and co-doping with appropriate REIs, which allows them to be used in many areas. Compounds with olivine structure crystallize in the orthorhombic system (sp. gr. *Pnma*, $Z = 4$), their structural and energy features have been studied in detail in the works of Russian and foreign authors [16, 17]. However, it is necessary to note some properties of $NaREGeO_4$ matrices that affect the optical properties of phosphors formed on their basis, in particular, the reduced phonon energy (~800 $cm^{-1}$), significant band gap value close to 6 eV [18], high crystal-chemical capacity of the lattice during isovalent substitutions of REI. Despite the high degree of ordering of the olivine structure with composition $NaYGeO_4$, the introduction of bismuth ions can lead to the formation of defects due to the presence of bismuth ions in various charge states: 2+, 3+, and 4+ in the system. This feature underlies the creation of phosphors with long afterglow, used in devices for data collection and storage. The presented data indicate the possibility of creating promising multifunctional phosphors based on $NaREGeO_4$ olivines with iso- and heterovalent substitution of $RE^{3+}$ ions.

In the presented work, the influence of the synthesis method (solid-phase and liquid-phase) on the spectral-luminescent properties of samples with composition $NaY_{0.975}Tm_{0.025}GeO_4$, possessing emission in the near-IR range (1100–2100 nm) when excited by radiation with $\lambda_{ex} = 808$ nm, was assessed. The influence of annealing conditions of germanates $NaGdGeO_4$, namely sintering in a standard muffle or microwave furnace, on morphological characteristics and optical properties in the UV region ($\lambda_{em} = 300–320$ nm, $\lambda_{ex} = 257$ nm) was considered. The optical characteristics of compounds $NaY_{0.975}Bi_{0.025}GeO_4$ and $NaY_{0.875}Bi_{0.025}Eu_{0.1}GeO_4$, possessing long afterglow in the UV and visible wavelength range (300–700 nm, $\lambda_{ex} = 298$ nm) [19, 20], were studied.

The obtained results allowed us to draw conclusions about possible ways to optimize methods for obtaining phosphors with olivine structure and their influence on morphological and spectral-luminescent properties.

## EXPERIMENTAL PART

For the synthesis of the research objects, $Na_2CO_3$ (99.9%), $Y_2O_3$ (99.99%), $Gd_2O_3$ (99.99%), $Eu_2O_3$ (99.99%), $Tm_2O_3$ (99.99%), $Bi_2O_3$ (99.99%) and $GeO_2$ (99.5%) were used as starting materials. The reagents were preliminarily brought to weight form by annealing at 650°C for 10 hours, which allowed the removal of moisture and $CO_2$ absorbed by the powders.

$NaGdGeO_4$, $NaY_{0.975}Tm_{0.025}GeO_4$, $NaY_{0.975}Bi_{0.025}GeO_4$ and $NaY_{0.875}Bi_{0.025}Eu_{0.1}GeO_4$ samples were obtained using liquid-phase ( **LP** ), specifically the citrate-nitrate method of precursor synthesis. A mixture of rare-earth oxides and $Na_2CO_3$, taken in stoichiometric amounts, was dissolved in diluted nitric acid $HNO_3$. $GeO_2$ oxide was dissolved separately in an aqueous solution of $NH_4OH$. The obtained solutions were mixed, after which citric acid $(CH_2)_2C(OH)(COOH)_3 \cdot 2H_2O$ was added as a complexing agent. The final solution was evaporated until precipitation. To remove organic impurities, the precursors were step-annealed at 650, 750, and 800 °C for 5 hours. The synthesis of the $NaY_{0.975}Tm_{0.025}GeO_4$ sample was additionally carried out using the solid-phase method ( **SP** ). Further thermal treatment of the obtained precursors was carried out under the conditions presented in Table 1. Three types of furnaces were used in the synthesis: a microwave furnace SVCh-laborant (Ural-Gefest, Russia), a muffle furnace with air atmosphere (SNOL, Lithuania), and a muffle furnace with argon atmosphere PTK-1.4-40 (Teplopribor, Russia). In the case of step annealing, intermediate grinding of the obtained phases was performed.

**Table 1.** Annealing conditions of the studied samples

| Annealing conditions | Sample form | $t$, ° °C | τ, h |
|---|---|---|---|
| $NaGdGeO_4$ | | | |
| Muffle furnace (MF) | Powder | 900, 1050, 1100 | 10, 25, 5 |
| Muffle furnace (MT) | Tablet | 900, 1050, 1100 | 10, 25, 5 |
| Microwave furnace (MP) | Powder | 900 | 3 |
| Microwave furnace (MT) | Tablet | 900 | 3 |
| $NaYGeO_4$ | | | |
| Muffle furnace | Tablet | 900, 1000, 1050 | 20, 20, 5 |
| $NaY_{0.975}Tm_{0.025}GeO_4$ | | | |
| Muffle furnace (after LF) | Tablet | 900, 1000, 1050 | 20, 20, 5 |
| Muffle furnace (after SF) | Tablet | 700, 800, 900, 1000, 1200 | 20 at each temperature |
| $NaY_{0.975}Bi_{0.025}GeO_4$, $NaY_{0.875}Bi_{0.025}Eu_{0.1}GeO_4$ | | | |
| Microwave furnace (M) | Tablet | 850 | 3 |
| Muffle furnace (M) | Tablet | 900, 1050, 1100 | 10, 20, 5 |
| Muffle furnace with argon atmosphere (MA) | Tablet | 1000 | 20 |

X-ray phase analysis of the obtained compounds was performed on a Stadi-P diffractometer (STOE, Germany) in Bragg-Brentano geometry. The scanning was

carried out in Cu $K_\alpha$-radiation in the angular range of 5°–70° with a step of 0.03°. Polycrystalline silicon with parameter $a$ = 5.43075(5) Å was used as an external standard. The refinement of lattice parameters was performed using the PowderCell 2.4 program [21]. The X-ray diffraction patterns of the obtained samples fully correspond to the data for $NaYGeO_4$ from the PDF2 database (ICDD), Card No. 01-088-1177. For full-profile refinement, data from [16] were used as the initial model. In the synthesized solid solutions, due to the proximity of crystalline radii at CN = 6 ($Gd^{3+}$ (1.078 Å), $Y^{3+}$ (1.040 Å), $Tm^{3+}$ (1.020 Å), $Bi^{3+}$ (1.17 Å), $Eu^{3+}$ (1.087 Å) [22]), isovalent substitution of trivalent yttrium with REI or $Bi^{3+}$ occurs. Corresponding model representations were included in the calculation.

Microstructural and morphological analyses were conducted using a Jeol JSM-6390 LA scanning electron microscope (Japan), equipped with an EDX attachment.

Adsorption isotherms were obtained by the static volumetric method on a Gemini VII 2390 V1.03 (USA) instrument. The obtained dependencies were described and specific surface area calculations were performed using the BET method based on nitrogen adsorption data.

For comparison of optical measurement results, all materials were converted to powder form. Luminescence spectra of samples with the same composition were recorded under identical conditions and normalized to unity.

Luminescence spectra of $NaY_{0.85}Tm_{0.15}GeO_4$ samples were obtained in the range of 900–2200 nm under excitation by a laser diode with $\lambda_{ex}$ = 808 nm ($P$ = 1200 mW, KLM-808-200-5, FTI-Optronic, Russia). The emission was recorded using an MDR-204 monochromator (LOMO-Photonics, Russia) and a FPU-FS PbS semiconductor detector (LOMO-Photonics, Russia). A diffraction grating of 600 lines/mm and an optical shutter with a modulation frequency of 200 Hz were used during the measurements.

The excitation and luminescence spectra of $NaGdGeO_4$ samples in the 200–800 nm range were recorded using a modular spectrophotometer, which included two

MDR-204 monochromators (LOMO-Photonics, Russia) with diffraction gratings of 1200 lines/mm, a BSI pulse counting unit (LOMO-Photonics, Russia), and a PMT R2949 (Hamamatsu). A Hamamatsu L-4279 xenon lamp was used as the radiation source.

The optical properties of $NaY_{0.975}Bi_{0.025}GeO_4$ and $NaY_{0.875}Bi_{0.025}Eu_{0.1}GeO_4$, including afterglow, were studied using a Varian Cary Eclipse spectrofluorometer, equipped with a 75 kW xenon lamp (pulse duration $\tau = 2$ μs, pulse frequency $\nu = 80$ Hz, wavelength resolution 0.5 nm; PMT R928). Measurements were performed using Varian software.

## RESULTS AND DISCUSSION

### *Synthesis results*

For each sample, depending on the chosen synthesis method, the duration and annealing temperature were established experimentally; the obtained values are given in Table 1. It was found that after the second stage of annealing in a muffle furnace, the diffraction patterns of the powders showed lines from impurity phases or a slight broadening of the peaks related to the target product, which is associated with its insufficient crystallization. The final synthesis temperature was selected in accordance with the phase diagram of olivines presented in works [23, 24]. The authors reported that at $t \geq 1260$°C, incongruent melting of olivines can occur; for this reason, the final synthesis temperature in the present study did not exceed this value. Despite the fact that annealing in argon flow is technologically more complex and requires greater economic costs, its use in the synthesis of $NaY_{0.975}Bi_{0.025}GeO_4$ and $NaY_{0.875}Bi_{0.025}Eu_{0.1}GeO_4$ made it possible to evaluate the influence of the external atmosphere on the afterglow of germanates. X-ray phase analysis established that single-phase samples of the specified compositions are formed during annealing at a temperature of 1000°C for 20 hours. Olivines $NaGdGeO_4$, $NaY_{0.975}Bi_{0.025}GeO_4$ and $NaY_{0.875}Bi_{0.025}Eu_{0.1}GeO_4$ were obtained as a result of a three-hour one-step microwave annealing at temperatures of

850-900°C. The heat treatment temperatures under microwave radiation for the latter compositions differed somewhat due to the different rare earth ions in the composition. Thus, microwave annealing of germanates with an olivine structure made it possible to reduce the synthesis temperature by 150-200°C and reduce its time to 3 hours.

*X-ray Diffraction Analysis Results*

According to X-ray diffraction data, the synthesized samples of $NaGdGeO_4$, $NaY_{0.975}Tm_{0.025}GeO_4$, $NaY_{0.975}Bi_{0.025}GeO_4$ and $NaY_{0.875}Bi_{0.025}Eu_{0.1}GeO_4$ crystallize in the orthorhombic system (space group *Pnma*, $Z = 4$). After the final annealing stage, no reflections from impurity phases were observed on the diffraction patterns of the samples (Fig. 1). The relative intensities of the peaks in the powder diffraction pattern of $NaGdGeO_4$ differ from the values for the standard sample of $NaYGeO_4$, which is explained by the larger amplitude of X-ray scattering by gadolinium atoms. This circumstance was taken into account when refining the X-ray patterns using the Rietveld method. The calculated unit cell parameters for all compounds are presented in Table S1.

*Surface Characteristics Investigation*

SEM images were obtained to study the surface morphology of the synthesized samples. The grains of $NaY_{0.975}Tm_{0.025}GeO_4$ LPF and SPF powders have predominantly irregular shape and form agglomerates (Fig. 2a, 2b). Since the particles of the sample obtained as a result of solid-phase synthesis were somewhat melted, it is not possible to determine the actual average particle size. However, such a study was conducted for the $NaGdGeO_4$ SH and MH matrix (Fig. 2c, 2d). The average grain size ( $r$ ) of $NaGdGeO_4$ SH was $r = 0.57 \pm 0.21$ μm, while for $NaGdGeO_4$ MH the particle size distribution was somewhat wider: $r = 0.68 \pm 0.37$ μm (Fig. 2d, 2e). Figure 2c clearly shows that, unlike the sample annealed in a standard muffle furnace, the sample after processing in a microwave oven consists of particles with a more regular shape, close to spherical. This was also observed in the SEM images of samples S (Fig. 2g), M (Fig. 2h), MA (Fig. 2i) of composition $NaY_{0.875}Bi_{0.025}Eu_{0.1}GeO_4$ similar to the composition

$NaY_{0.975}Bi_{0.025}GeO_4$. A more detailed comparison of the SEM images presented in Fig. 2e, 2g shows that the particle agglomerates of samples annealed in argon atmosphere are less melted, which is probably a consequence of the shorter annealing time.

The obtained data indicate that prolonged annealing at temperatures >1000°C leads to melting of particles and formation of agglomerates. At the same time, in the case of germanate $NaY_{0.975}Tm_{0.025}GeO_4$ prepared by solid-state reaction, it was necessary since the single-phase product was obtained only after heat treatment at 1200°C. Thus, it was not possible to evaluate the influence of selected synthesis methods on the shape and size of $NaY_{0.975}Tm_{0.025}GeO_4$ powder particles. No significant effect of annealing in argon atmosphere on the morphology of $NaY_{0.975}Bi_{0.025}GeO_4$ and $NaY_{0.875}Bi_{0.025}Eu_{0.1}GeO_4$ samples was observed.

Since microwave annealing should lead to increased sintering density and, consequently, decreased sample porosity, it was reasonable to compare the specific surface area after annealing in muffle and microwave furnaces. Thus, adsorption isotherms were studied for all samples of $NaGdGeO_4$ composition (Fig. 3). The calculated values of specific surface area $S_{sp}$ indicate low porosity of the studied materials. It is noteworthy that the specific surface area of $NaGdGeO_4$ SR and SP samples is slightly larger than that of MW and MP samples of $NaGdGeO_4$ composition (Fig. 3), which is probably due to the lower dispersity of the latter.

*Evaluation of the synthesis conditions influence on optical characteristics of germanates*

Since the wavelength ranges in which the luminescence of the studied compounds was observed differ significantly from each other, which is associated with the different nature of luminescent REI, the optical properties of germanates will be considered separately.

*Influence of the Synthesis Method on Luminescent Characteristics of $NaY_{0.975}Tm_{0.025}GeO_4$*

Luminescence spectra of LF and SF samples of $NaY_{0.975}Tm_{0.025}GeO_4$ were obtained in the wavelength range of 1100–2100 nm at $\lambda_{ex}$ = 808 nm (Fig. 4a). The presented spectra contain two broad bands in the ranges of 1300–1600 nm and 1600–2100 nm, caused respectively by transitions $^3H_4 \rightarrow {}^3F_4$ and $^3F_4 \rightarrow {}^3H_6$ of the $Tm^{3+}$ ion (Fig. 4b). In paper [25], it is shown that de-excitation from the state $^3H_4$ can proceed in two ways: through cascade relaxation and migration-accelerated cross-relaxation to the state $^3F_4$ (in this case, $Tm^{3+}$ ions play the role of both activator and sensitizer). The transition $^3F_4 \rightarrow {}^3H_6$ is also migration-accelerated (Fig. 4b).

The spectra of LF and SF samples have identical profiles, but the intensity of the latter's lines is significantly lower. This is probably due to the larger size of particle agglomerates in the SF sample and, consequently, to a smaller specific surface area. In other words, the number of thulium ions on the surface exposed to excitation radiation is smaller, which affects the probability of their excitation and, as a result, the intensity of the subsequent luminescence.

*Influence of Annealing Conditions on $NaGdGeO_4$*

Luminescence $_4$ germanates annealed under various conditions were recorded at $\lambda_{em}$ = 315 nm (Fig. 5a). The peak in the range of 255-260 nm is due to the $4f$-$4f$ transition of the $Gd^{3+}$ ion from the ground state $^8S_{7/2}$ to the excited state $^6D_{9/2}$ (Fig. 5c). Photoluminescence spectra of the samples were obtained under excitation at $\lambda_{ex}$ = 257 nm. The spectra (Fig. 5b) show a line with a maximum at 315 nm, corresponding to the transition $^6P_{7/2} \rightarrow {}^8S_{7/2}$ of the $Gd^{3+}$ ion.

The spectral profiles of all $NaGdGeO_4$ samples have a similar shape. However, there is a notable difference in the luminescence intensity of samples annealed in muffle and microwave furnaces. The luminescence of CT and CP samples is almost 1.5 times more intense, which is probably due to their greater dispersity and less melted grains, as evidenced by SEM images. The luminescence of the MT sample was somewhat higher than that of MP, therefore, in the case of annealing in a muffle furnace, the shape of the sample being sintered plays a more significant role. The lesser influence of

sample shape during microwave annealing is explained by the higher density and rate of grain sintering [10-12].

### *Influence of Annealing Conditions on the Afterglow Duration of $NaY_{0.975}Bi_{0.025}GeO_4$ and $NaY_{0.875}Bi_{0.025}Eu_{0.1}GeO_4$ Samples*

There are several models explaining the mechanism of luminescence in systems doped with $Bi^{3+}$ ions [26 , 27]. The most common are the concepts proposed by the authors [28, 29], according to which electron transfer between neighboring bismuth ions is a common phenomenon for phosphors doped with $Bi^{3+}$. The transfer mechanism is realized through the formation of a $Bi^{3+}$–$Bi^{3+}$ pair. When exposed to radiation with a wavelength $\lambda_{ex} = 298$ nm, an electron transitions to the excited state $^3P_1$ of the $Bi^{3+}$ ion, then it transfers to a neighboring bismuth ion, forming an electron-hole pair $Bi^{2+}$ – $Bi^{4+}$ [28]. The sublevels of $Bi^{2+}$ act as electron traps. The $^2P_{1/2}$ state of $Bi^{2+}$ ions in doped $NaYGeO_4$ has a depth of $0.85 \pm 0.5$ eV relative to the conduction band, thus, the phosphor $NaYGeO_4$: $Bi^{3+}$ can store the energy of exciting radiation with a wavelength $\lambda_{ex} = 298$ nm [29]. After turning off the excitation radiation source, the electron is released from the $^2P_{1/2}$ sublevel of $Bi^{2+}$ ions and additional excitation of the system occurs, which leads to the appearance of an afterglow band in the range of 300–500 nm. According to literature data, for some phosphors, the described process can last up to 28 hours [27].

Figure 6a, 6b shows the excitation and photoluminescence spectra of samples C, M, MA of composition $NaY_{0.875}Bi_{0.025}Eu_{0.1}GeO_4$. The excitation spectra at $\lambda_{em} = 410$ nm have two broad lines in the ranges of 200–250 and 275–350 nm, associated with transitions $^1S_0 \rightarrow {}^1P_1$ and $^1S_0 \rightarrow {}^3P_1$ of the $Bi^{3+}$ ion, respectively. The different effects of annealing conditions on the described processes are noteworthy. When exciting the samples in the band corresponding to the transition $^1S_0 \rightarrow {}^1P_1$, the luminescence intensity was similar for all three samples and reached a maximum for sample C, annealed in a microwave oven, as in the case of $NaGdGeO_4$. A diametrically opposite picture is observed when excitation is carried out in the band associated with

the transition $^1S_0 \rightarrow {}^3P_1$; in this case, sample M has the maximum luminescence intensity. Probably, this fact is due to the morphological properties of the $NaY_{0.875}Bi_{0.025}Eu_{0.1}GeO_4$(M) sample, namely the larger particle size as a result of longer sintering. As a consequence, the probability of forming a bismuth pair is higher in such samples. A possible scheme of energy transfer between $Bi^{2+}$, $Bi^{3+}$ and $Eu^{3+}$ ions is demonstrated in Figure 6e . $Bi^{2+}$ levels, acting as traps, are located close to the $^3P_1$ level of $Bi^{3+}$ ions, and their deactivation likely contributes to the excitation of $Bi^{3+}$ ions. Thus, it can be assumed that samples $NaY_{0.975}Bi_{0.025}GeO_4$ and $NaY_{0.875}Bi_{0.025}Eu_{0.1}GeO_4$, synthesized in a muffle furnace in air (M), will exhibit longer afterglow. The effect of defects on the $^1P_1$ state is minimal due to its distance from the $Bi^{2+}$ sublevel. The low content of $Bi^{2+}$ ions does not allow experimental determination and correlation of the number of defects under different annealing conditions.

The photoluminescence spectra of the samples consist of a broad band in the range of 300–500 nm, corresponding to the $^3P_1 \rightarrow {}^1S_0$ transition of $Bi^{3+}$ ion, and a set of lines in the range of 530–680 nm, caused by $4f$–$4f$ -transitions of $Eu^{3+}$ ion. The influence of annealing conditions on the intensity of the band in the short-wavelength region is similar to that described earlier for excitation spectra. The intensity of the lines due to transitions in $Eu^{3+}$ depends weakly on the annealing conditions.

At the final stage of the work, the afterglow of $NaY_{0.975}Bi_{0.025}GeO_4$ and $NaY_{0.875}Bi_{0.025}Eu_{0.1}GeO_4$ samples was studied. The measurements were carried out using a Varian Cary Eclipse spectrofluorimeter. The phosphors were excited with radiation at a wavelength of $\lambda_{ex} = 298$ nm for 2 minutes. It should be noted that for $NaY_{0.875}Bi_{0.025}Eu_{0.1}GeO_4$ samples, prolonged afterglow was not observed, which, according to [29], is associated with a shallower depth of traps. The evaluation of the influence of annealing conditions on the afterglow was carried out on $NaY_{0.975}Bi_{0.025}GeO_4$ samples (Fig. 6c, 6d). As expected, the germanate $NaY_{0.975}Bi_{0.025}GeO_4$ M, annealed in a muffle furnace, has the most intense afterglow. The duration of the afterglow for this phosphor was 20 minutes after turning off the excitation source, for samples MA and C of the

same composition - 15 and 13 minutes, respectively. The latter is indirect confirmation of a higher defect concentration in sample M compared to MA and C.

## CONCLUSION

Germanates $NaGdGeO_4$, $NaY_{0.975}Tm_{0.025}GeO_4$, $NaY_{0.975}Bi_{0.025}GeO_4$ and $NaY_{0.875}Bi_{0.025}Eu_{0.1}GeO_4$ were synthesized using various methods with different annealing options in the final stages of synthesis. It has been demonstrated that thermal annealing in a microwave oven helps to reduce the final synthesis temperature of the compounds by 150-200°C and significantly shortens the synthesis duration. A significant influence of prolonged high-temperature annealing in a standard muffle furnace on the morphological characteristics of powders was discovered, in particular, grain melting was revealed for samples $NaY_{0.975}Tm_{0.025}GeO_4$ TF and $NaY_{0.875}Bi_{0.025}Eu_{0.1}GeO_4$ M, MA. The influence of synthesis conditions on the luminescent properties of compounds $NaY_{0.975}Tm_{0.025}GeO_4$, $NaY_{0.975}Bi_{0.025}GeO_4$ and $NaY_{0.875}Bi_{0.025}Eu_{0.1}GeO_4$, emitting in different wavelength ranges, was considered. According to the obtained data, the phosphor $NaGdGeO_4$, annealed in a microwave oven, has the highest luminescence intensity. However, in the case of germanates $NaY_{0.975}Bi_{0.025}GeO_4$ and $NaY_{0.875}Bi_{0.025}Eu_{0.1}GeO_4$, whose excitation efficiency is directly related to the number of defect states formed during the synthesis process, the luminescence intensity was maximum for samples annealed in a muffle furnace for a long time.

## FUNDING

The study of the influence of synthesis conditions on the morphological and luminescent characteristics of $NaGdGeO_4$ and $NaY_{0.975}Tm_{0.025}GeO_4$ samples was carried out within the framework of the state assignment of the ISSC UB RAS (theme No. 124020600024-5). The study of the luminescent characteristics of $NaY_{0.975}Bi_{0.025}GeO_4$ and $NaY_{0.875}Bi_{0.025}Eu_{0.1}GeO_4$ samples was carried out with the support of the Russian Science Foundation (grant No. 23-73-10090), https://rscf.ru/project/23-73-10090/

## CONFLICT OF INTEREST

The authors declare no conflict of interest.

## ADDITIONAL INFORMATION

The online version contains supplementary materials available at https://doi.org/

## REFERENCES


1. *Riya Dey a, Vineet Kumar Rai* // Dalton Trans . 2014. V. 43. P. 111. https://doi.org/10.1039/C3DT51773J
2. *Scholle K., Lamrini S., Koopmann P. et al.* // Front. Guided Wave Opt. Optoelectron. 2010. V. 13. № 5. https://doi.org/10.5772/39538
3. *Sordillo L.A., Yang Pu , Pratavieira S. et al.* // J. Biomed. Opt. 2014. V. 19. P. 56004. https://doi.org/10.1117/1.JBO.19.5.056004
4. *Hao Zhang, Yang Wei, Xiao Huanga et al.* // J. Lumin . 2019. V. 207. P. 137. https://doi.org/10.1016/j.jlumin.2018.10.117
5. *Lipina O.A., Surat L.L., Melentsova A.A. et al.* // Phys. Solid State. 2021. V. 7. P. 944. https://doi.org/10.21883/FTT.2021.07.51046.050
6. *Lipina O.A., Spiridonova T.S., Baklanova Ya.V. et al.* // Russ. J. Inorg. Chem. 2023. V. 68. P. 603. https://doi.org/ 10.31857/S0044457X22601973
7. *Gang Xiong, Zhanping Zhang, Yuhong Qi* // Prog. Org. Coat. 2022. V. 170 . P. 106965. https://doi.org/10.1016/j.porgcoat.2022.106965
8. *Gyrdasova O.I., Kalinkin M.O., Aulov D.A. et al.* // Russ. J. Inorg. Chem. 2023. V. 68. № 2. P. 277. https://doi.org/ 10.31857/S0044457X22601754
9. *Dahiya M.S., Tomer V.K., Duhan S.* // Appl. Nanocompos. Mater. Drug Delivery. 2008. V. 31. P. 737. https://doi.org/10.1016/B978-0-12-813741-3.00032-7
10. *Lenczewska K., Szymański D., Hreniak D.* // Mater. Res. Bull. 2022. V. 154. P. 111940. https://doi.org/10.1016/j.materresbull.2022.111940
11. *Tang H., Tang Y., Xiao M. et al.* // Colloids Surf., A. 2022. V. 651. P. 129564. https://doi.org/10.1016/j.colsurfa.2022.129564

12. *Lau K.S., Hassan Z., Lim W.F. et al.* // Mater. Chem. Phys. 2022. V. 292. P. 126649. https://doi.org/10.1016/j.matchemphys.2022.126649

13. *Melentsova A.A., Lipina O.A., Chufarov A.Yu. et al.* // J. Solid State Chem. 2023. V. 322. P. 123946. https://doi.org/10.1016/j.jssc.2023.123946

14. *Latshaw A.M., Wilkins B.O., Chance W.M. et al.* // J. Solid State Sci. 2016. V. 51. P. 59. https://doi.org/10.1016/j.solidstatesciences.2015.11.009

15. *Tyutyunnik A.P., Leonidov I.I., Surat L.L. et al.* // J. Solid State Chem. 2013. V. 197. P. 447.

16. *Dudka A.P., Kaminskii A.A., Simonov V.I.* // Phys. Status Solidi . 1986. V. 93. № 2. P. 495. https:// doi.org/10.1002/pssa.2210930212

17. *Melkozerova M.A., Artyomov M.Yu., Enyashin A.N. et al.* // J. Solid State Chem. 2022. V. 315. P. 123475. https://doi.org/10.1016/j.jssc.2022.123475

18. *Ermakova L.V., Leonidov I.I.* // Mater. Lett. 2018. V. 233. P. 39. https://doi.org/10.1016/j.matlet.2018.08.125

19. *Lin Liu , Kexin Yu , Liyan Ming et al.* // J. Rare Earths . 2022. V. 40. № 9. P. 1424. https://doi.org/10.1016/j.jre.2021.04.017

20. *Wenxiang Wang , Zhenyu Sun , Xiaoyang He et al.* // J. Mater. Chem . 2017. V. 5. № 17. P. 4310. https://doi.org/10.1039/C6TC05598B

21. *Kraus W., Nolze G.* // J. Appl. Crystallogr. 1996. V. 29. P. 301.

22. *Shannon R.D.* // Acta Crystallogr., Sect. A. 1976. V. 32. P. 751.

23. *Litvin A.Yu., Kuzyura A.V.* // Geochem. Int . 2021. V. 59. № 9 . P. 813. https://doi.org/ 10.31857/S0016752521080045

24. *Koseva I. , Nikolov V. , Petrova N. et al.* // Thermochim. Acta. 2016. V. 646. P. 1. https://doi.org/10.1016/j.tca.2016.11.004

25. *Melentsova A.A. , Lipina O.A. , Melkozerova M.A. et al.* // Ceram. Int . 2023. V. 59. № 11 . P. 18681. https://doi.org/10.1016/j.ceramint.2024.02.356

26. *Junpeng Xue, Hyeon Mi Noh, Byung Chun Choi et al.* // Chem. Eng. J. 2020. V. 383. P. 122861. https://doi.org/10.1016/j.cej.2019.122861

27. *Lin Liu, Kexin Yu, Liyan Ming et al.* // J. Rare Earths. 2022. V. 40. № 9. P. 1424. https://doi.org/10.1016/j.jre.2021.04.017

28. *Awater R.H.P., Dorenbos P.* // J. Lumin. 2017. V. 188. P. 487.

http://dx.doi.org/10.1016/j.jlumin.2017.05.011

29. *Lyu T., Dorenbos P.* // Chem. Mater. 2020. V. 32. № 3. P. 1192. https://dx.doi.org/10.1021/acs.chemmater.9b04341

## FIGURE CAPTIONS

**Fig. 1.** XRPD patterns of $NaGdGeO_4$ MP, $NaY_{0.975}Tm_{0.025}GeO_4$ SM, $NaY_{0.875}Bi_{0.025}Eu_{0.1}GeO_4$ M, $NaYGeO_4$ and $NaYGeO_4$ powders synthesized in this work together with the XRPD pattern of the standard $NaYGeO_4$ sample, PDF2 No. 01-088-1177.

**Fig. 2.** SEM images of the powders $NaY_{0.975}Tm_{0.025}GeO_4$ SM (a) and SSM (b), $NaGdGeO_4$ MT (c), FT (d), $NaY_{0.875}Bi_{0.025}Eu_{0.1}GeO_4$ M (g), F (h), FA (i); Particle size distribution of the $NaGdGeO_4$ of samples MT (e), FT (f).

**Fig. 3.** Adsorption isotherms of the $NaGdGeO_4$ samples FP, FT, MP and MT.

**Fig. 4.** a) Luminescence spectra ($\lambda_{ex}$ = 808 nm) of $NaY_{0.975}Tm_{0.025}GeO_4$ samples SM and SSM, b) Simplified energy level diagrams of $Tm^{3+}$ ions, as well as the main excitation, energy transfer and radiative processes.

**Fig. 5.** Luminescence excitation (a) and emission (b) spectra of the $NaGdGeO_4$ samples: MP, MT, FP and FT. Simplified energy level diagrams of $Gd^{3+}$ ions, as well as the main excitation, energy transfer and radiative processes (c).

**Fig. 6.** Luminescence excitation (a) and emission (b) spectra of the $NaY_{0.875}Bi_{0.025}Eu_{0.1}GeO_4$ samples: M, F and FA. Persistent luminescence spectra of the $NaY_{0.975}Bi_{0.025}GeO_4$ phosphors: M, F and FA, obtained immediately after switching off 298 nm excitation radiation (exposure duration was two minutes) (c). Persistent luminescence spectra of the $NaY_{0.975}Bi_{0.025}GeO_4$ FA sample, obtained after different time after switching off the excitation radiation (d). Simplified energy level diagrams of $Bi^{3+}$, $Eu^{3+}$ ions, as well as the main excitation, energy transfer and radiative processes (e) in $NaY_{0.875}Bi_{0.025}Eu_{0.1}GeO_4$ phosphor.

**Table 1.** Annealing conditions and sample designation

| Furnace type | Sample form | Temperature $T$, °C | Time $t$, h. |
|---|---|---|---|

| | | | |
|---|---|---|---|
| $NaGdGeO_4$ | | | |
| Muffle furnace ( *FP* ) | powder | 900, 1050, 1100 | 10, 25, 5 |
| Muffle furnace ( *FT* ) | tablet | 900, 1050, 1100 | 10, 25, 5 |
| Microwave furnace ( *MP* ) | powder | 900 | 3 |
| Microwave furnace ( *MT* ) | tablet | 900 | 3 |
| $NaYGeO_4$ | | | |
| Muffle furnace | tablet | 900, 1000, 1050 | 20, 20, 5 |
| $NaY_{0.975}Tm_{0.025}GeO_4$ | | | |
| Muffle furnace (SM *)* | tablet | 900, 1000, 1050 | 20, 20, 5 |
| Muffle furnace (SSM *)* | tablet | 700, 800, 900, 1000, 1200 | 20 at all T |
| $NaY_{0.975}Bi_{0.025}GeO_4$, $NaY_{0.875}Bi_{0.025}Eu_{0.1}GeO_4$ | | | |
| Microwave furnace ( *M* ) | tablet | 850 | 3 |
| Muffle furnace ( *F* ) | tablet | 900, 1050, 1100 | 10, 20, 5 |
| Argon atmosphere muffle furnace ( *FA* ) | tablet | 1000 | 20 |

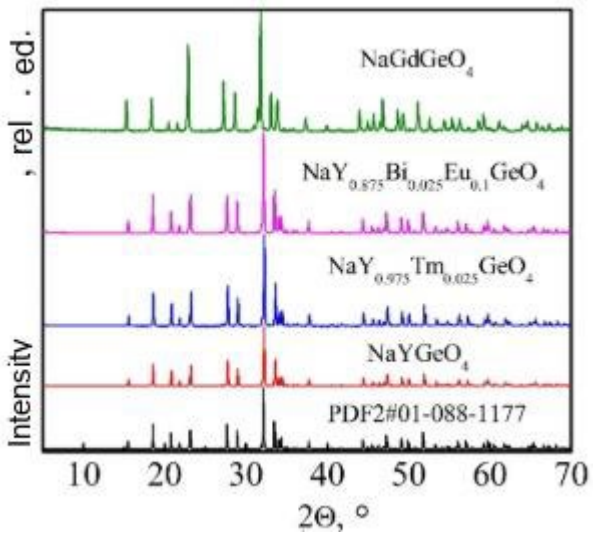


Fig. 1. Melentsova.

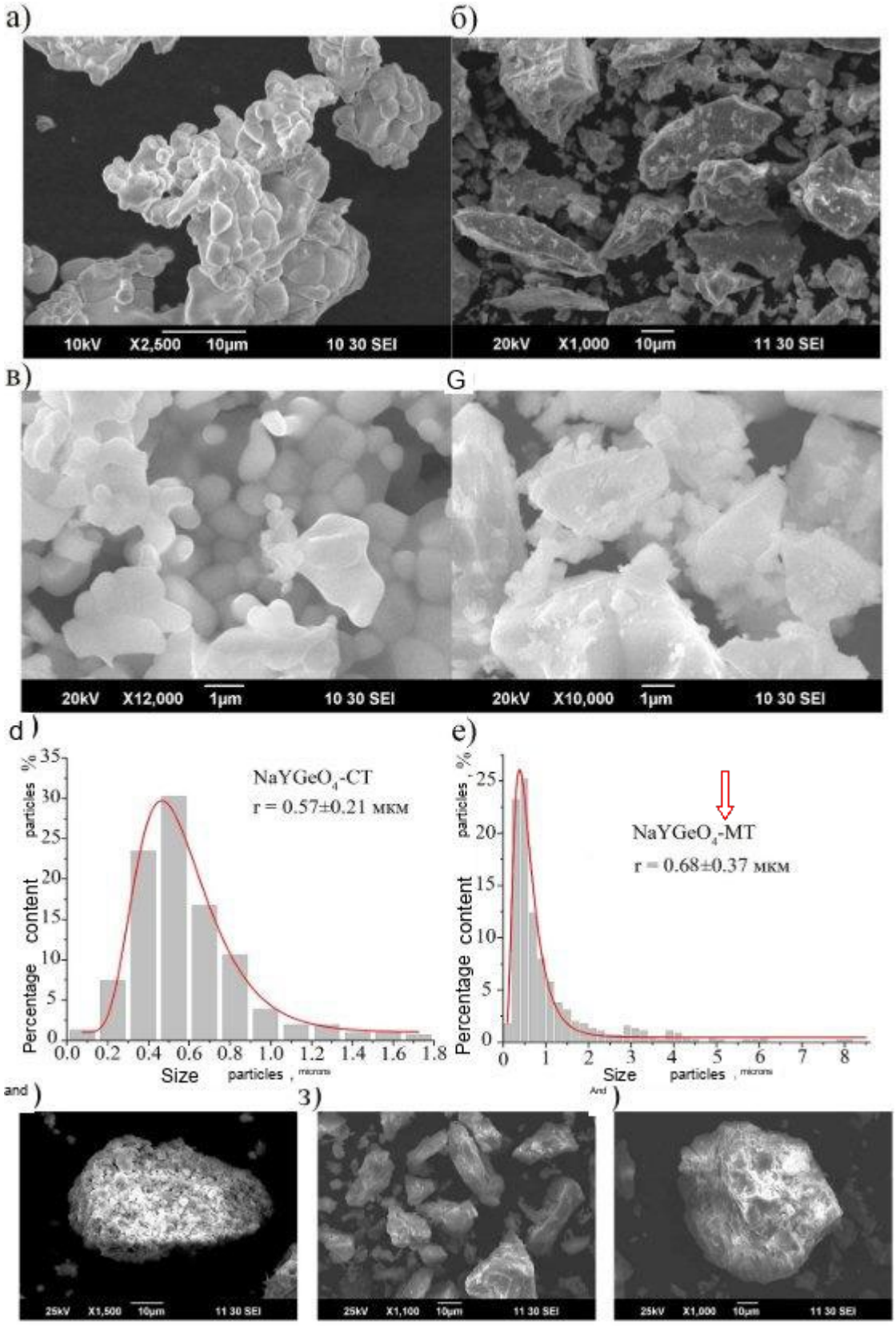
а)
б)
10kV X2,500 10µm 10 30 SEI
20kV X1,000 10µm 11 30 SEI
в)
G
20kV X12,000 1µm 10 30 SEI
20kV X10,000 1µm 10 30 SEI
d)
e)
NaYGeO4-CT
r = 0.57±0.21 мкм
NaYGeO4-MT
r = 0.68±0.37 мкм
Percentage content, %
Size particles, microns
and)
3)
And)
25kV X1,500 10µm 11 30 SEI
25kV X1,100 10µm 11 30 SEI
25kV X1,000 10µm 11 30 SEI

Fig. 2. Melentsova.

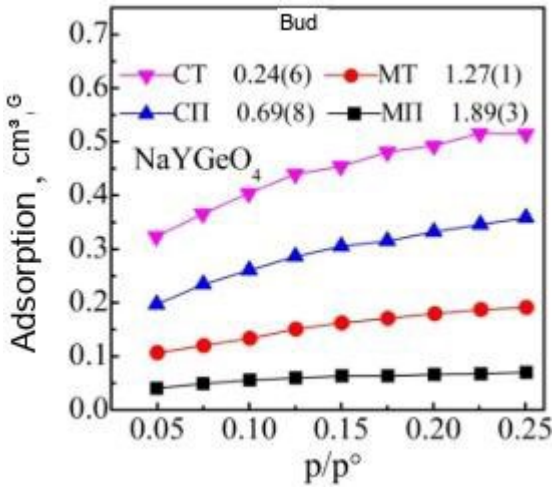


Fig. 3. Melentsova.

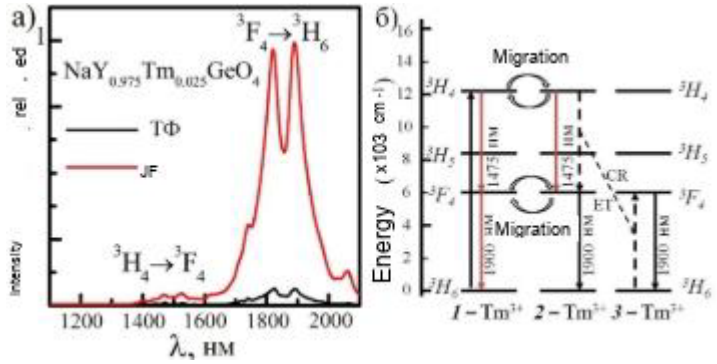


Fig. 4. Melentsova.

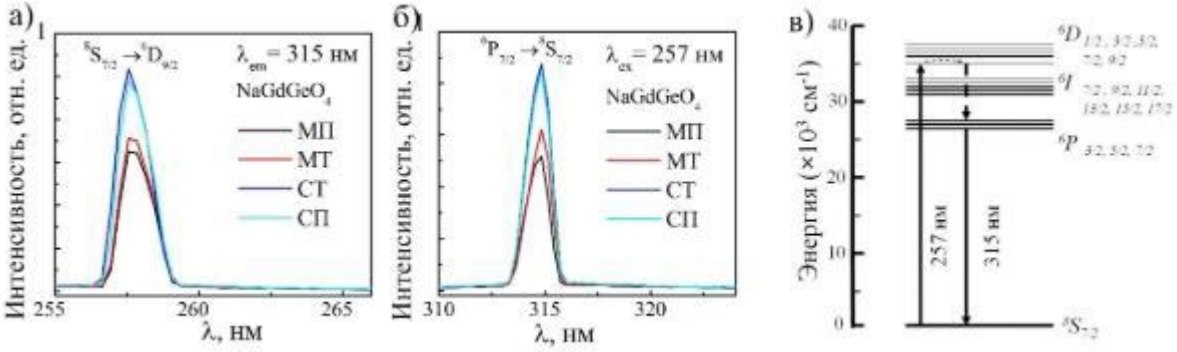


Fig. 5. Melentsova.

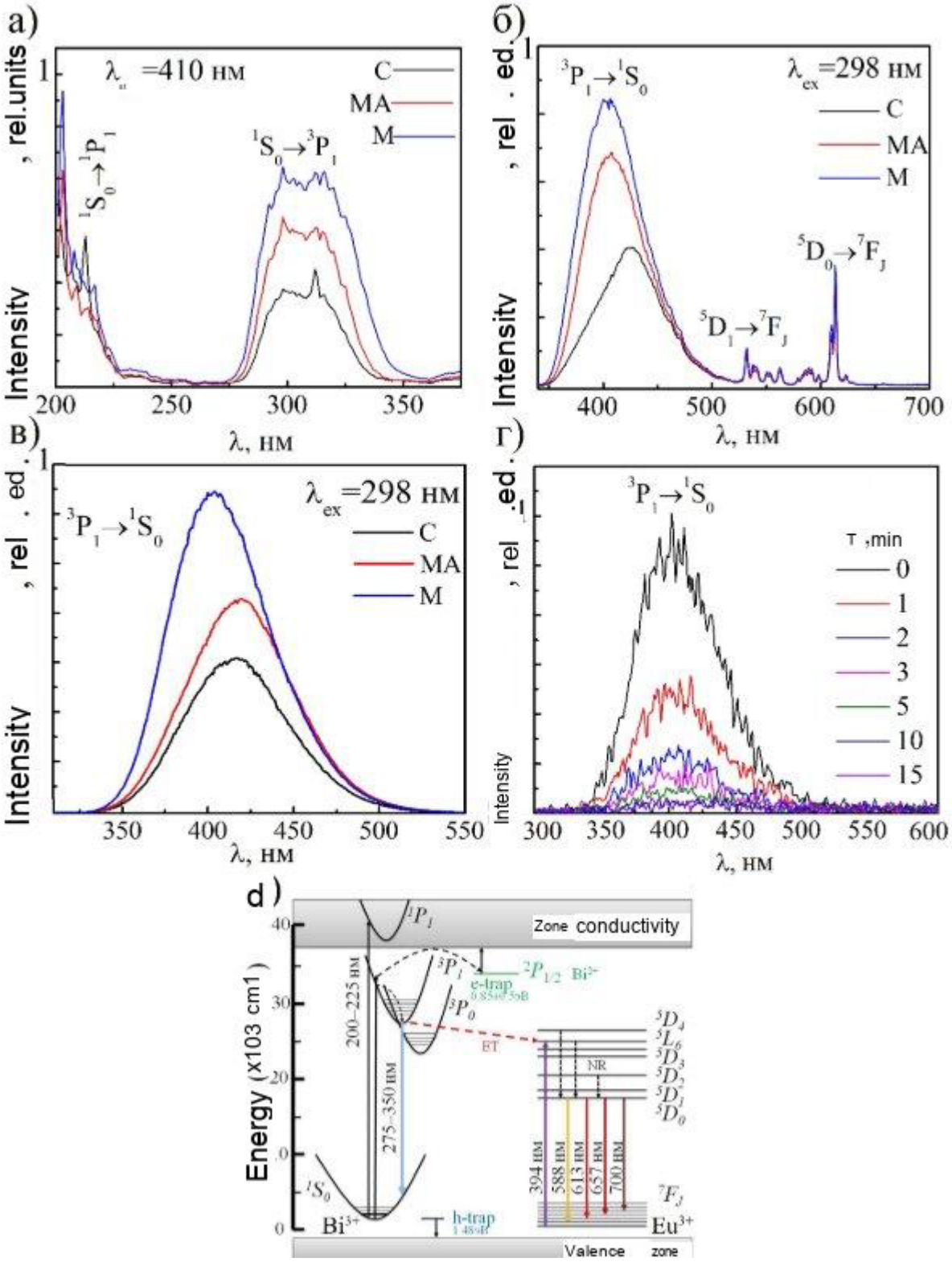


Fig. 6. Melentsova.